Symplectic integrators in sub-Riemannian geometry: the Martinet case

Monique Chyba, Ernst Hairer, Gilles Vilmart

INSTITUT NATIONAL DE RECHERCHE EN INFORMATIQUE ET EN AUTOMATIQUE

Symplectic integrators in sub-Riemannian geometry: the Martinet case

Monique Chyba — Ernst Hairer — Gilles Vilmart

N° 6017

Novembre 2006

Thème NUM

ISSN 0249-6399 ISRN INRIA/RR--6017--FR+ENG

INRIA
RENNES

Symplectic integrators in sub-Riemannian geometry: the Martinet case

Monique Chyba *, Ernst Hairer †, Gilles Vilmart † ‡

Thème NUM — Systèmes numériques
Projet Ipso

Rapport de recherche n° 6017 — Novembre 2006 — 10 pages

Abstract: We compare the performances of symplectic and non-symplectic integrators for the computation of normal geodesics and conjugate points in sub-Riemannian geometry at the example of the Martinet case. For this case study we consider first the flat metric, and then a one parameter perturbation leading to non integrable geodesics. From our computations we deduce that near the abnormal directions a symplectic method is much more efficient for this optimal control problem. The explanation relies on the theory of backward error analysis in geometric numerical integration.

Key-words: sub-Riemannian geometry, Martinet, abnormal geodesic, symplectic integrator, backward error analysis.

This work was partially supported by the Fonds National Suisse, project No. 200020-109158 and by the National Science Foundation grant DMS-030641.

* University of Hawaii, Department of Mathematics, 2565 Mc Carthy the Mall, Honolulu 96822, Hawaii
† Université de Genève, Section de mathématiques, 2-4 rue du Lièvre, CP 64, 1211 Genève 4, Switzerland
‡ INRIA Rennes, projet IPSO, Campus de Beaulieu, 35042 Rennes Cedex, France

Unité de recherche INRIA Rennes
IRISA, Campus universitaire de Beaulieu, 35042 Rennes Cedex (France)
Téléphone : +33 2 99 84 71 00 — Télécopie : +33 2 99 84 71 71

Intégrateurs symplectiques en géométrie sous-riemannienne: le problème de Martinet

Résumé : On compare les performances d'intégrateurs symplectiques et non symplectiques pour le calcul de géodésiques normales et de points conjugués dans un exemple sous-riemannien, le problème de Martinet. On étudie le problème d'abord avec une métrique plate, puis avec une perturbation à un paramètre conduisant à des géodésiques non intégrables. De cette étude, on déduit que proche des directions anormales, une méthode symplectique est bien plus efficace pour ce problème de contrôle optimal. L'explication repose sur la théorie de l'analyse rétrograde en intégration numérique géométrique.

Mots-clés : géométrie sous-riemannienne, Martinet, geodésique anormale, intégrateur symplectique, analyse rétrograde

Introduction

This paper is a follow-up to a series of articles that were published in the past decades, see [1, 2] and the references therein. There, the authors provide an analytic study of the singularity of the sub-Riemannian sphere in the Martinet case. They complement their analysis with numerical computations to represent the geodesics and the sphere, and to locate the conjugate points. The integrator used for these computations is an explicit Runge-Kutta method of order 5(4). The goal of the present paper is to compare the performances of a symplectic integrator versus a non-symplectic one for this optimal control problem. To be more precise, let (U, Δ, g) be a sub-Riemannian structure where U is an open neighborhood of R^3, Δ a distribution of constant rank 2 and g a Riemannian metric. When Δ is a contact distribution, there are no abnormal geodesics, and a non-symplectic integrator is as efficient as a symplectic one. However, when the distribution is taken as the kernel of the Martinet one-form, we show that a symplectic integrator is much more efficient for the computation of the normal geodesics and their conjugate points near the abnormal directions.

Both problems, the Martinet flat case and a non integrable perturbation, are introduced in Sect. 1 together with the corresponding differential equations. Numerical experiments with an explicit Runge–Kutta method and with the symplectic Störmer–Verlet method are presented in Sect. 2 and illustrated with figures. Close to abnormal geodesics, the results are quite spectacular. For a relatively large step size, the symplectic integrator provides a solution with the correct qualitative behavior and a satisfactory accuracy, while for the same step size the non-symplectic integrator gives a completely wrong numerical solution with an incorrect behavior, particularly for the non integrable case. The explanation relies on the theory of backward error analysis (Sect. 3). It is related to the geometric structure of the problem and its solutions.

1 A Martinet type sub-Riemannian structure

In this section, we briefly recall some results of [1] for a sub-Riemannian structure (U, Δ, g). Here, U is an open neighborhood of the origin in R^3 with coordinates $q = (x, y, z)$, and g is a Riemannian metric for which a graduated normal form, at order 0, is $g = (1 + \alpha y)dx^2 + (1 + \beta x + \gamma y)dy^2$. The distribution Δ is generated by the two vector fields $F_1 = \frac{\partial}{\partial x} + \frac{y^2}{2}\frac{\partial}{\partial z}$ and $F_2 = \frac{\partial}{\partial y}$ which correspond to $\Delta = \ker \omega$ where $\omega = dz - \frac{y^2}{2}dx$ is the Martinet canonical one-form. To this distribution we associate the affine control system

$$\dot{q} = u_1(t)F_1(q) + u_2(t)F_2(q),$$

where $u_1(t), u_2(t)$ are measurable bounded functions which act as controls.

We consider two cases, the Martinet flat case $g = dx^2 + dy^2$, an integrable situation, and a one parameter perturbation $g = dx^2 + (1 + \beta x)^2 dy^2$ for which the set of geodesics is non integrable.

1.1 Geodesics

It follows from the Pontryagin maximum principle, see [1, 2], that the normal geodesics corresponding to $g = dx^2 + (1 + \beta x)^2 dy^2$ are solutions of an Hamiltonian system

$$\dot{q} = \frac{\partial H}{\partial p}(q, p), \qquad \dot{p} = -\frac{\partial H}{\partial q}(q, p), \tag{1}$$

where $q = (x, y, z)$ is the state, $p = (p_x, p_y, p_z)$ is the adjoint state, and the Hamiltonian is

$$H(q, p) = \frac{1}{2}\left(\left(p_x + p_z\frac{y^2}{2}\right)^2 + \frac{p_y^2}{(1 + \beta x)^2}\right).$$

In other words, the normal geodesics are solutions of the following equations:

$$\begin{aligned}
\dot{x} &= p_x + p_z\frac{y^2}{2} & \dot{p}_x &= \frac{\beta\, p_y^2}{(1 + \beta x)^3} \\
\dot{y} &= \frac{p_y}{(1 + \beta x)^2} & \dot{p}_y &= -\left(p_x + p_z\frac{y^2}{2}\right)p_z y \\
\dot{z} &= \left(p_x + p_z\frac{y^2}{2}\right)\frac{y^2}{2} & \dot{p}_z &= 0.
\end{aligned} \tag{2}$$

Notice that the variables z and p_z do not influence the other equations (except via the initial value $p_z(0)$), so that we are actually confronted with a Hamiltonian system in dimension four. For the Martinet flat case ($\beta = 0$), the interesting dynamics takes place in the two-dimensional space of coordinates (y, p_y). The Hamiltonian is

$$H(y, p_y) = \frac{p_y^2}{2} + \frac{1}{2}\Big(p_x + p_z \frac{y^2}{2}\Big)^2,$$

where p_x and p_z have to be considered as constants. This is a one-degree of freedom mechanical system with a quartic potential. For $p_x < 0 < p_z$, the Hamiltonian $H(y, p_y)$ has two local minima at $(y = \pm\sqrt{-2p_x/p_z},\ p_y = 0)$, which correspond to stationary points of the vector field. In this case, the origin $(y = 0,\ p_y = 0)$ is a saddle point.

Whereas normal geodesics correspond to oscillating motion, it is shown in [1, 2] that the abnormal geodesics are the lines $z = z_0$ contained in the plane $y = 0$. For the considered metrics, the abnormal geodesics can be obtained as projections of normal geodesics, we say that they are not strictly abnormal. In [2], the authors introduce a geometric framework to analyze the singularities of the sphere in the abnormal direction when $\beta \neq 0$. See also [3, 4] for a precise description of the role of the abnormal geodesics in sub-Riemannian geometry in the general non-integrable case, i.e., when the abnormal geodesics can be strict. The major result of these papers is the proof that the sub-Riemannian sphere is not sub-analytic because of the abnormal geodesics.

Interesting phenomena arise when the normal geodesics are close to the separatrices connecting the saddle point. Therefore, we shall consider in Sect. 2 the computation of normal geodesics with $y(0) = 0$ and $p_y(0) > 0$ but small.

1.2 Conjugate points

For the Hamiltonian system (1) we consider the exponential mapping

$$\exp_{q_0,t} : p_0 \longmapsto q(t, q_0, p_0)$$

which, for fixed $q_0 \in R^3$, is the projection $q(t, q_0, p_0)$ onto the state space of the solution of (1) starting at $t = 0$ from (q_0, p_0). Following the definition in [1] we say that the point q_1 is conjugate to q_0 along $q(t)$ if there exists (p_0, t_1), $t_1 > 0$, such that $q(t) = \exp_{q_0,t}(p_0)$ with $q_1 = \exp_{q_0,t_1}(p_0)$, and the mapping $\exp_{q_0,t_1}$ is not an immersion at p_0. We say that q_1 is the first conjugate point if t_1 is minimal. First conjugate points play a major role when studying optimal control problems since it is a well known result that a geodesic is not optimal beyond the first conjugate point.

For the numerical computation of the first conjugate point, we compute the solution of the Hamiltonian system (1) together with its variational equation,

$$\dot{y} = J^{-1}\nabla H(y), \qquad \dot{\Psi} = J^{-1}\nabla^2 H(y)\Psi. \tag{3}$$

Here, $y = (q, p)$ and J is the canonical matrix for Hamiltonian systems. It can be shown that for Runge-Kutta methods, the derivative of the numerical solution with respect to the initial value, $\Psi_n = \partial y_n/\partial y_0$, is the result of the same numerical integrator applied to the augmented system (3), see [5, Lemma VI.4.1]. Here, the matrix

$$\Psi = \begin{pmatrix} \partial q/\partial q_0 & \partial q/\partial p_0 \\ \partial p/\partial q_0 & \partial p/\partial p_0 \end{pmatrix}$$

has dimension 6×6. The conjugate points are obtained when $\partial q/\partial p_0$ becomes singular, i.e., $\det(\partial q/\partial p_0) = 0$.

2 Comparison of symplectic and non-symplectic integrators

For the numerical integration of the Hamiltonian system (1), where we rewrite $\frac{\partial H}{\partial q}(q, p) = H_q(q, p)$ and $\frac{\partial H}{\partial p}(q, p) = H_p(q, p)$, we consider two integrators of the same order 2:

- a non-symplectic, explicit Runge–Kutta discretization, denoted RK2 (see [5, Sect. II.1.1]),

$$\begin{aligned} q_{n+1/2} &= q_n + \frac{h}{2}H_p(q_n, p_n) & p_{n+1/2} &= p_n - \frac{h}{2}H_q(q_n, p_n) \\ q_{n+1} &= q_n + hH_p(q_{n+1/2}, p_{n+1/2}) & p_{n+1} &= p_n - hH_q(q_{n+1/2}, p_{n+1/2}) \end{aligned} \tag{4}$$

- the symplectic Störmer–Verlet scheme (see e.g. [5, Sect. VI.3]),

$$\begin{aligned} p_{n+1/2} &= p_n - \frac{h}{2} H_q(q_n, p_{n+1/2}) \\ q_{n+1} &= q_n + \frac{h}{2}\Big(H_p(q_n, p_{n+1/2}) + H_p(q_{n+1}, p_{n+1/2})\Big) \\ p_{n+1} &= p_{n+1/2} - \frac{h}{2} H_q(q_{n+1}, p_{n+1/2}) \end{aligned} \tag{5}$$

where $q_n = (x_n, y_n, z_n)$ and $p_n = (p_{x,n}, p_{y,n}, p_{z,n})$. Here, $q_n \approx q(nh)$, $p_n \approx p(nh)$ and h is the step size.

For the computation of the conjugate points, we apply the numerical methods to the variational equation (3). Notice that only the partial derivatives with respect to p_0 have to be computed. Conjugate points are then detected when $\det(\partial q_n/\partial p_0)$ changes sign. We approximate them by linear interpolation which introduces an error of size $\mathcal{O}(h^2)$. This is comparable to the accuracy of the chosen integrators which are both of second order.

Remark 2.1 The Störmer–Verlet scheme (5) is implicit in general. A few fixed point iterations yield the numerical solution with the desired accuracy. Notice however that the method becomes explicit in the Martinet flat case $\beta = 0$. One simply has to compute the components in a suitable order, for instance $p_{x,n+1}$, $p_{z,n+1}$, $p_{y,n+1/2}$, y_{n+1}, x_{n+1}, z_{n+1}, $p_{y,n+1}$.

2.1 Martinet flat case

We consider first the flat case $\beta = 0$ in the Hamiltonian system (2). As initial values we choose (cf. [1])

$$x(0) = y(0) = z(0) = 0, \quad p_x(0) = \cos\theta_0, \quad p_y(0) = \sin\theta_0, \quad p_z(0) = 10, \quad \text{where} \quad \theta_0 = \pi - 10^{-3}, \tag{6}$$

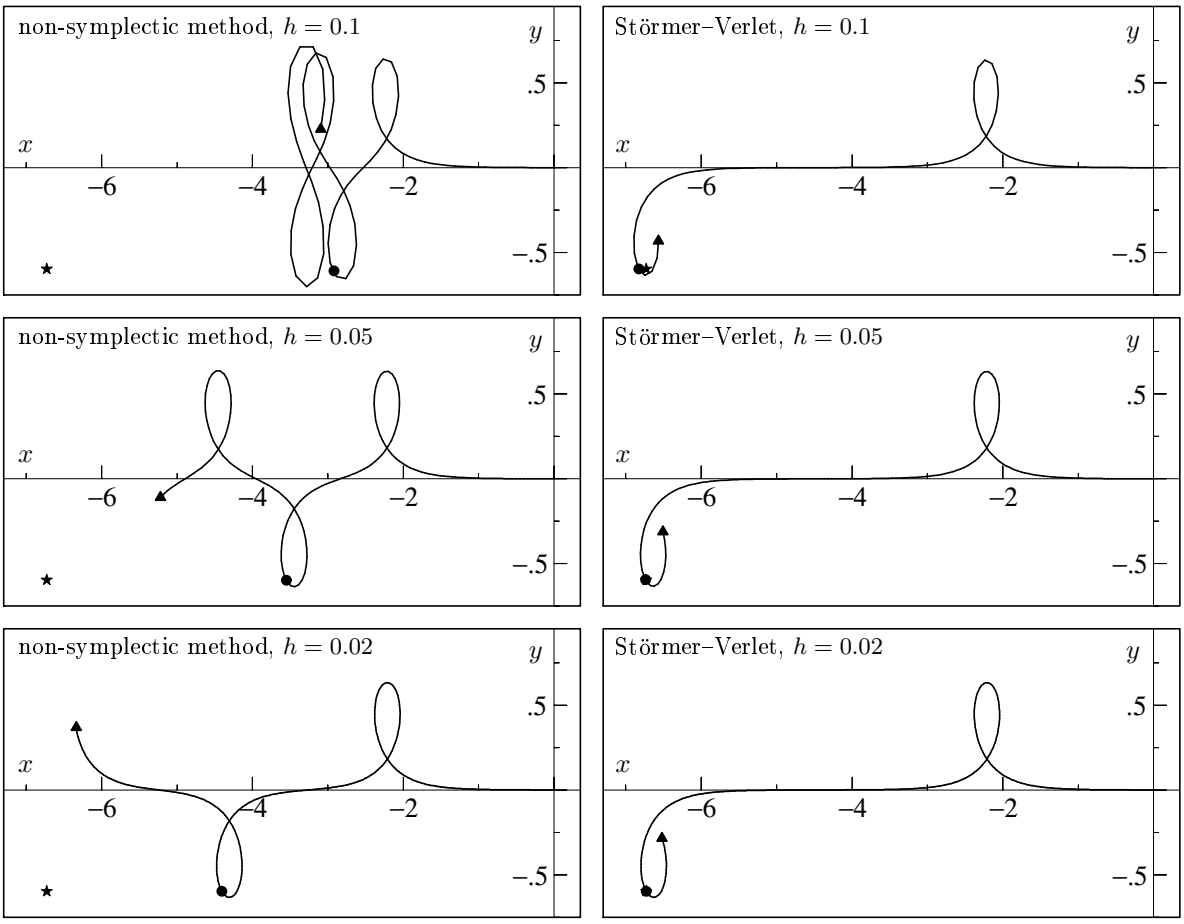

Figure 1: Trajectories in the (x, y)-plane for the flat case $\beta = 0$.

so that we start close to an abnormal geodesics, and we integrate the system over the interval $[0, 9]$.

Figure 1 displays the projection onto the (x, y)-plane of the numerical solution obtained with different step sizes h by the two integrators. The initial value is at the origin, and the final state is indicated by a triangle. The circles represent the first conjugate point detected along the numerical solution, while the stars give the position of the first conjugate point on the exact solution of the problem. There is an enormous difference between the two numerical integrators. The symplectic (Störmer–Verlet) method (5) provides a qualitatively correct solution already with a large step size $h = 0.1$, and it gives an excellent approximation for step sizes smaller than $h = 0.05$. On the other hand, the non-symplectic, explicit Runge–Kutta method (4) gives completely wrong results, and step sizes smaller than 10^{-3} are needed to provide an acceptable solution. An explanation of the different behavior of the two integrators will be given in Sect. 3 below.

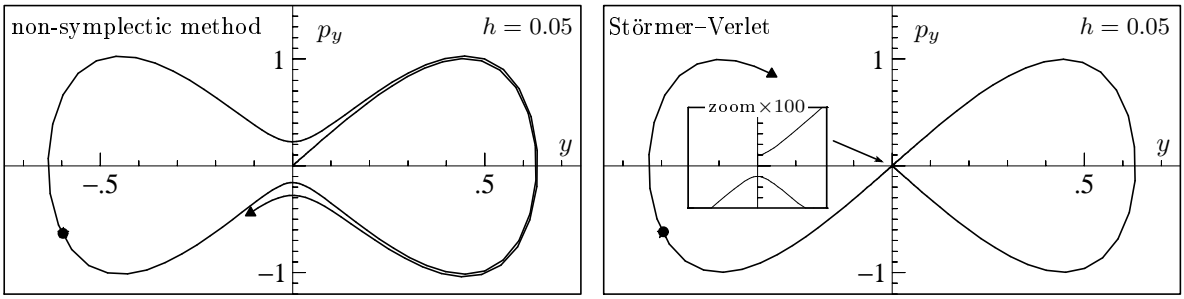

Figure 2: Phase portraits in the (y, p_y)-plane for the flat case $\beta = 0$.

As noticed in Sect. 1, the normal geodesics in the flat case are determined by a one-degree of freedom Hamiltonian system in the variables y and p_y. We therefore show in Figure 2 the projection onto the (y, p_y)-space of the solutions previously computed with step size $h = 0.05$. The exact solution starts at $(0, \sin\theta_0)$ above the saddle point, turns around the positive stationary point, crosses the p_y-axis at $(0, -\sin\theta_0)$, turns around the negative stationary point, and then continues periodically. The numerical approximation by the non-symplectic method covers more than one and a half periods, whereas the Störmer–Verlet and the exact solution cover less than one period for the time interval $[0, 9]$. Since the conjugate point is not very sensible with respect to perturbations in the initial value for p_y, the (y, p_y) coordinates of the conjugate point obtained by the non-symplectic integrator are rather accurate, but the corresponding integration time is completely wrong.

Table 1 lists the conjugate time obtained with the two integrators using various step sizes. There is a significant difference between the two methods. We can see that with the Störmer–Verlet method (5) a step size of order $h = 10^{-2}$ provides a solution with 4 correct digits. A step size a 100 times smaller is needed to get the same precision with the non-symplectic method.

2.2 Non integrable perturbation

For our next numerical experiment we choose the perturbation parameter $\beta = -10^{-4}$ in the differential equation (2). We consider the same initial values and the same integration interval as in Sect. 2.1. The exact solution is no longer periodic and, due to the fact that β is chosen negative, its projection onto the (y, p_y)-space slowly spirals inwards around the positive stationary point (see right picture in Figure 4).

Figures 3 and 4 and Table 1 display the numerical results obtained by the two integrators for the differential equation (2) with $\beta = -10^{-4}$. The interpretation of the symbols (triangles, circles, and stars) is the same as before. The excellent behavior of the symplectic integrator is even more spectacular than in the flat case, and the pictures obtained for the Störmer–Verlet method agree extremely well with the exact solution. The

Table 1: Accuracy for the first conjugate time.

Martinet flat case		
h	RK2	Verlet
10^{-1}	4.504945	8.504716
10^{-2}	6.748262	8.416622
10^{-3}	8.360340	8.416412
10^{-4}	8.416349	8.416410
exact solution: $t_1 \approx 8.416409$		

Non integrable situation		
h	RK2	Verlet
10^{-1}	4.511294	4.883832
10^{-2}	7.380322	4.877056
10^{-3}	4.877183	4.876998
10^{-4}	4.876997	4.876997
exact solution: $t_1 \approx 4.876997$		

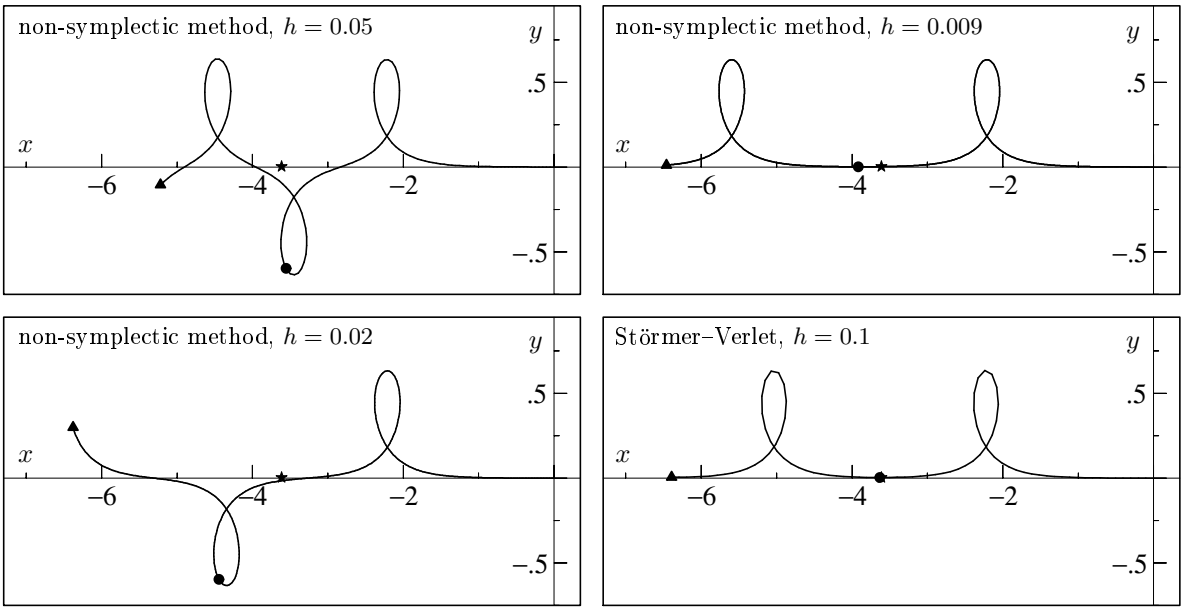

Figure 3: Trajectories in the (x, y)-plane for the non integrable case $\beta = -10^{-4}$.

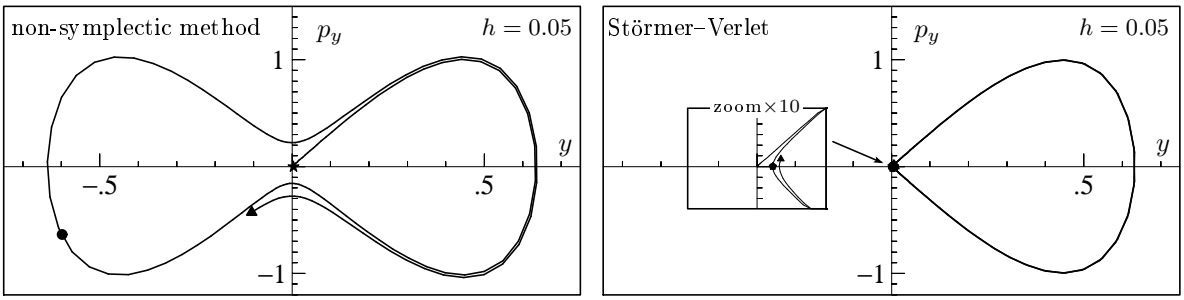

Figure 4: Phase portraits in the (y, p_y)-plane for the non integrable case $\beta = -10^{-4}$.

non-symplectic method gives qualitatively wrong solutions for step sizes larger than $h = 0.01$. In the (y, p_y)-space it alternatively spirals around the right and left stationary points whereas the exact solution spirals only around the positive stationary point. In contrast to the Martinet flat case, the conjugate point obtained by the non-symplectic method is here wrong also in the (y, p_y)-space.

2.3 An asymptotic formula on the first conjugate time in the Martinet flat case

Now that we have shown the efficiency of symplectic integrators, we can make more precise the asymptotic behaviour studied in [1]. For the initial values of (6) and $\beta = 0$, consider the ratio

$$R = \frac{t_1\sqrt{p_z}}{3K(k)},$$

where t_1 is the first conjugate time for the normal geodesic, and $K(k)$ is an elliptic integral of the first kind,

$$K(k) = \int_0^{\pi/2} \frac{1}{\sqrt{1 - k^2 \sin^2 u}} du, \qquad k = \sin(\theta_0/2).$$

By studying analytic solutions for the normal geodesics, it is proved in [1] that this ratio satisfies the inequality $2/3 \leq R \leq 1$. It follows from a rescaling of the equations (2) that R is independent of p_z.

In Figure 5, we represent the values of $1 - R$ as a function of $\varepsilon = \pi - \theta_0$, for various initial values θ_0. The numerical results indicate that the ratio R depends on θ_0, and $R \longrightarrow 1^-$ slowly for $\theta_0 \longrightarrow \pi^-$.

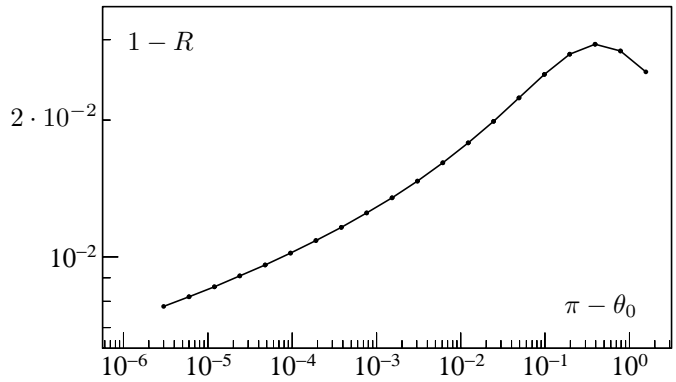

Figure 5: Illustration of the asymptotic behaviour of R (Störmer–Verlet scheme with step size $h = 10^{-4}$).

3 Backward error analysis

The theory of backward error analysis is fundamental for the study of geometric integrators and it is treated in much detail in the monographs of Sanz-Serna & Calvo [7], Hairer, Lubich & Wanner [5, Chap. IX], and Leimkuhler & Reich [6]. It allows us to explain the numerical phenomena encountered in the previous section.

3.1 Backward error analysis and energy conservation

We briefly present the main ideas of backward error analysis for the study of symplectic integrators, see [5, Chap. IX]. Consider a system of differential equations

$$\dot{y} = f(y), \quad y(0) = y_0 \tag{7}$$

and a numerical integrator $y_{n+1} = \Phi_h(y_n)$ of order p. The idea is to search for a *modified differential equation* written as a formal series in powers of the step size h,

$$\dot{\widetilde{y}} = \widetilde{f}(\widetilde{y}) = f(\widetilde{y}) + h^p f_{p+1}(\widetilde{y}) + h^{p+1} f_{p+2}(\widetilde{y}) + \dots, \tag{8}$$

such that $y_n = \widetilde{y}(t_n)$ for $t_n = nh$, $n = 0, 1, 2, \dots$, in the sense of formal power series. The motivation of this approach is that it is often easier to study the modified equation (8) than directly the numerical solution.

What makes backward error analysis so important for the study of symplectic integrators is the fact that, when applied to a Hamiltonian system $\dot{y} = J^{-1}\nabla H(y)$, the modified equation (8) has the same structure $\dot{\widetilde{y}} = J^{-1}\nabla \widetilde{H}(\widetilde{y})$ with a *modified Hamiltonian*

$$\widetilde{H}(y) = H(y) + h^p H_{p+1}(y) + h^{p+1} H_{p+2}(y) + \dots \ .$$

However, the series usually diverges, so a truncation at a suitable order $N(h)$ is necessary,

$$\widetilde{H}(y) = H(y) + h^p H_{p+1}(y) + \dots + h^{N-1} H_N(y).$$

This truncation induces an error that can be made exponentially small, by choosing $N(h) \sim C/h$, see [5, Theorem IX.8.1]. More precisely, we have that for $t_n = nh$ and $h \to 0$,

$$\widetilde{H}(y_n) = \widetilde{H}(y_0) + \mathcal{O}(t_n e^{-h_0/h}). \tag{9}$$

as long as the numerical solution $\{y_n\}$ stays in a compact set. On intervals of length $\mathcal{O}(e^{h_0/2h})$, the modified Hamiltonian $\widetilde{H}(y)$ is thus exactly conserved up to exponentially small terms.

3.2 Backward error analysis for the Martinet problem

Symplectic integrators are successfully applied in the long-time integration of Hamiltonian systems, for instance in astronomy (e.g. the Outer Solar System over 100 million years [5, Sect. I.2.4]), or in molecular dynamics [6, Chap. 11]. Here the situation is quite different because we are interested in the numerical integration of Hamiltonian systems on relatively short time intervals.

3.2.1 Martinet flat case

Consider the Martinet problem (2) in the flat case $\beta = 0$. Its interesting dynamics takes place in the (y, p_y) plane, and it is not influenced by the other variables (only by their initial values). We put $\eta = (y, p_y)$, and we denote by $f(\eta)$ the Hamiltonian vector field composed by the corresponding two equations of (2). For a numerical integrator of order $p = 2$, the associated modified differential equation has the form

$$\dot{\widetilde{\eta}} = f(\widetilde{\eta}) + h^2 f_3(\widetilde{\eta}) + \mathcal{O}(h^3). \tag{10}$$

Consider first the symplectic Störmer–Verlet method. It follows from Sect. 3.1 that its modified differential equation is Hamiltonian, and from (9) that the modified Hamiltonian $\widetilde{H}(\eta)$ is preserved up to exponentially small terms along the numerical solution. This implies that the numerical solution remains exponentially close to a periodic orbit in the (y, p_y)-space. The critical point ($y=0$, $p_y=0$) is a saddle point also for the modified differential equation (because the origin is stationary also for the numerical solution and thus for the modified equation). Therefore, any numerical solution starting close to the origin has to come back to it after turning around one of the stationary points. The minimal distance to the origin will always stay the same (see the zoom in Figure 2). This explains the good behavior of symplectic integrators.

For the non-symplectic integrator, the term $h^2 f_3(\eta)$ is not Hamiltonian. Therefore the solution of the modified differential equation (and hence also the numerical solution) is no longer periodic. In fact, it spirals outwards and after surrounding the first stationary point, the numerical solution does not approach the saddle point sufficiently close, which induces a faster dynamics as can be observed in Figures 1 and 2. This causes a huge error, because close to the saddle point the numerical solution is most sensible to errors.

3.2.2 Non integrable perturbation

In this case, the argument in the comparison of symplectic and non-symplectic integrators is very similar to the discussion of the Van der Pol's equation in [5, Sect. XII.1]. For $\beta \neq 0$ (non integrable perturbation), the dynamics takes place in the four dimensional space with variables $\eta = (x, y, p_x, p_y)$. In this space the system (2) becomes

$$\dot{\eta} = f(\eta) + \beta g(\eta)$$

where $f(\eta)$ is the Hamiltonian vector field corresponding to $\beta = 0$ and $g(y) = \mathcal{O}(1)$ depends smoothly on β. Here, the modified equation becomes

$$\dot{\widetilde{\eta}} = f(\widetilde{\eta}) + \beta g(\widetilde{\eta}) + h^2 f_3(\widetilde{\eta}) + \mathcal{O}(h^3 + \beta h^2),$$

where the perturbation term $h^2 f_3(\eta)$ is the same as for the Martinet flat case.

For the symplectic integrator, the perturbation $\beta g(\eta)$ has the same effect for the original problem as for $\dot{\widetilde{\eta}} = f(\widetilde{\eta}) + h^2 f_3(\widetilde{\eta}) + \ldots$. This explains the correct qualitative behavior for small h and small β. There is no restriction on the step size h compared to the size of β.

For the non-symplectic integrator, each of the perturbation terms $\beta g(\eta)$ and $h^2 f_3(\eta)$ destroys the periodic orbits in the subsystem for the (y, p_y) variables, and the dominant one will determine the behavior of the numerical solution. Only when $h^2 \ll |\beta|$, the numerical solution will catch the correct dynamics of the problem. In Figures 3 and 4, where $\beta = -10^{-4}$, this condition is not satisfied for $h \geq 10^{-2}$. Since β is chosen small and negative, the two perturbation terms are conflicting. The term $\beta g(\eta)$ causes the solution to spiral around the positive stationary point, whereas the term $h^2 f_3(\eta)$ causes it to spiral alternatively around both stationary points. For too large step sizes the qualitative behavior of the non-symplectic integrator (4) is thus completely wrong.

Remark 3.1 The problem (2) with $\beta = 0$ has a lot of symmetries. In the (y, p_y)-space the orbits are symmetric with respect to the y-axis and also with respect to the p_y-axis. If we apply a symmetric numerical integrator (not necessarily symplectic), it is possible to prove the same qualitative behavior as for the symplectic Störmer–Verlet method. This follows from the fact that the solution of the modified equation (numerical orbit) corresponding to a symmetric method has the same symmetry properties as the exact flow (see [5, Sect. IX.2] for precise statements). Consequently, in the (y, p_y) plane and for $\beta = 0$, the solution will stay exponentially near to a closed orbit, as it is the case for symplectic integrators. In the non integrable case, the good behavior of symmetric methods can be explained as in Sect. 3.2.2 for symplectic methods.

References

[1] A.A. Agrachev, B. Bonnard, M. Chyba, and I. Kupka. Sub-Riemannian sphere in Martinet flat case. *ESAIM/COCV (Control, Optimisation and Calculus of Variations)*, pp. 377-448, 1997.

[2] B. Bonnard, M. Chyba, and I. Kupka. Non Integrable Geodesics in SR-Martinet Geometry. *Proceedings of the 1997 Summer Research Institute on Differential Geometry and Control*, pp. 119-13, 1999.

[3] B. Bonnard, G. Launay, and E. Trelat. The transcendence needed to compute the sphere and wave front in Martinet SR-geometry. *J. Math. Sci., New York 103, 6*, pp. 688-708, 2001.

[4] B. Bonnard and E. Trelat. On the role of abnormal minimizers in SR-geometry. *Ann. Fac. Sci. Toulouse 6, X, 3*, pp. 405-491, 2001

[5] E. Hairer, C. Lubich, and G. Wanner. *Geometric Numerical Integration. Structure-Preserving Algorithms for Ordinary Differential Equations.* Springer Series in Computational Mathematics 31, Second Edition, Springer-Verlag, Berlin, 2006.

[6] B. Leimkuhler and S. Reich. *Simulating Hamiltonian Dynamics.* Cambridge Monographs on Applied and Computational Mathematics 14, Cambridge University Press, Cambridge, 2004.

[7] J. M. Sanz-Serna and M. P. Calvo. *Numerical Hamiltonian Problems.* Chapman & Hall, London, 1994.

Contents

1 A Martinet type sub-Riemannian structure **3**
1.1 Geodesics 3
1.2 Conjugate points 4

2 Comparison of symplectic and non-symplectic integrators **4**
2.1 Martinet flat case 5
2.2 Non integrable perturbation 6
2.3 An asymptotic formula on the first conjugate time in the Martinet flat case 7

3 Backward error analysis **8**
3.1 Backward error analysis and energy conservation 8
3.2 Backward error analysis for the Martinet problem 8
3.2.1 Martinet flat case 9
3.2.2 Non integrable perturbation 9

Unité de recherche INRIA Rennes
IRISA, Campus universitaire de Beaulieu - 35042 Rennes Cedex (France)

Unité de recherche INRIA Futurs : Parc Club Orsay Université - ZAC des Vignes
4, rue Jacques Monod - 91893 ORSAY Cedex (France)
Unité de recherche INRIA Lorraine : LORIA, Technopôle de Nancy-Brabois - Campus scientifique
615, rue du Jardin Botanique - BP 101 - 54602 Villers-lès-Nancy Cedex (France)
Unité de recherche INRIA Rhône-Alpes : 655, avenue de l'Europe - 38334 Montbonnot Saint-Ismier (France)
Unité de recherche INRIA Rocquencourt : Domaine de Voluceau - Rocquencourt - BP 105 - 78153 Le Chesnay Cedex (France)
Unité de recherche INRIA Sophia Antipolis : 2004, route des Lucioles - BP 93 - 06902 Sophia Antipolis Cedex (France)

Éditeur
INRIA - Domaine de Voluceau - Rocquencourt, BP 105 - 78153 Le Chesnay Cedex (France)
http://www.inria.fr
ISSN 0249-6399